Review of Scientific Instruments

RESEARCH ARTICLE | OCTOBER 24 2023

Ultra-thin polymer foil cryogenic window for antiproton deceleration and storage

B. M. Latacz ; B. P. Arndt ; J. A. Devlin ; S. R. Erlewein ; M. Fleck ; J. I. Jäger ; P. Micke ; G. Umbrazunas ; E. Wursten ; F. Abbass; D. Schweitzer; M. Wiesinger ; C. Will ; H. Yildiz ; K. Blaum ; Y. Matsuda ; A. Mooser ; C. Ospelkaus ; C. Smorra ; A. Sótér ; W. Quint ; J. Walz ; Y. Yamazaki ; S. Ulmer

Rev. Sci. Instrum. 94, 103310 (2023)
https://doi.org/10.1063/5.0167262

Review of Scientific Instruments ARTICLE pubs.aip.org/aip/rsi

Ultra-thin polymer foil cryogenic window for antiproton deceleration and storage

Cite as: Rev. Sci. Instrum. 94, 103310 (2023); doi: 10.1063/5.0167262
Submitted: 11 July 2023 • Accepted: 17 August 2023 •
Published Online: 24 October 2023

B. M. Latacz,[1,2,a] B. P. Arndt,[3,4] J. A. Devlin,[1,2] S. R. Erlewein,[2,3] M. Fleck,[2,5] J. I. Jäger,[1,2,3] P. Micke,[1,2,3] G. Umbrazunas,[2,6] E. Wursten,[2] F. Abbass,[7] D. Schweitzer,[7] M. Wiesinger,[3] C. Will,[3] H. Yildiz,[7] K. Blaum,[3] Y. Matsuda,[5] A. Mooser,[3] C. Ospelkaus,[8,9] C. Smorra,[2,7] A. Sótér,[6] W. Quint,[4] J. Walz,[7,10] Y. Yamazaki,[2] and S. Ulmer[2,11]

AFFILIATIONS

[1]CERN, Esplanade des Particules 1, 1217 Meyrin, Switzerland
[2]RIKEN, Ulmer Fundamental Symmetries Laboratory, 2-1 Hirosawa, Wako, Saitama 351-0198, Japan
[3]Max-Planck-Institut für Kernphysik, Saupfercheckweg 1, D-69117 Heidelberg, Germany
[4]GSI-Helmholtzzentrum für Schwerionenforschung GmbH, Planckstraße 1, D-64291 Darmstadt, Germany
[5]Graduate School of Arts and Sciences, University of Tokyo, 3-8-1 Komaba, Meguro, Tokyo 153-0041, Japan
[6]Eidgenössische Technische Hochschule Zürich, John-von-Neumann-Weg 9, 8093 Zürich, Switzerland
[7]Institut für Physik, Johannes Gutenberg-Universität, Staudinger Weg 7, D-55099 Mainz, Germany
[8]Institut für Quantenoptik, Leibniz Universität, Welfengarten 1, D-30167 Hannover, Germany
[9]Physikalisch-Technische Bundesanstalt, Bundesallee 100, D-38116 Braunschweig, Germany
[10]Helmholtz-Institut Mainz, Johannes Gutenberg-Universität, Staudingerweg 18, D-55128 Mainz, Germany
[11]Heinrich-Heine-Universität Düsseldorf, Universitätsstrasse 1, D-40225 Düsseldorf, Germany

[a]**Author to whom correspondence should be addressed:** barbara.latacz@cern.ch

ABSTRACT

We present the design and characterization of a cryogenic window based on an ultra-thin aluminized biaxially oriented polyethylene terephthalate foil at $T < 10$ K, which can withstand a pressure difference larger than 1 bar at a leak rate $<1 \times 10^{-9}$ mbar l/s. Its thickness of ~1.7 μm makes it transparent to various types of particles over a broad energy range. To optimize the transfer of 100 keV antiprotons through the window, we tested the degrading properties of different aluminum coated polymer foils of thicknesses between 900 and 2160 nm, concluding that 1760 nm foil decelerates antiprotons to an average energy of 5 keV. We have also explicitly studied the permeation as a function of coating thickness and temperature and have performed extensive thermal and mechanical endurance and stress tests. Our final design integrated into the experiment has an effective open surface consisting of seven holes with a diameter of 1 mm and will transmit up to 2.5% of the injected 100 keV antiproton beam delivered by the Antiproton Decelerator and Extra Low ENergy Antiproton ring facility of CERN.

I. INTRODUCTION

In many areas of physics, chemistry, or engineering, there is a need to separate ultra-high vacuum from high-pressure regions while nevertheless allowing the transfer of particles between the two sectors. Examples are physics experiments that use gaseous or liquid targets,[1] plasma-based particle acceleration,[2–4] trapping of antiprotons,[5–11] ion cooling,[12,13] or bio-mechanical applications where control over the types of particles that go through the membrane is required.[14–16] The goal of separating high and low pressure sectors is usually achieved either through differential pumping or by using thin, transparent vacuum windows for the incident particles. The main advantage of differential pumping is that the emittance of the particle beam can be conserved; however, this approach usually requires considerable technical effort, and the achievable pressure difference is quite limited. In contrast, using transparent vacuum windows for particles in a certain energy spectrum provides much

better vacuum conditions and is technically more efficient to implement; however, this technology causes significant particle beam distortions and limits the available particle flux.

In the Baryon Antibaryon Symmetry experiment (BASE),[5] conducted at the Antiproton Decelerator (AD) and Extra Low ENergy Antiproton (ELENA) ring antimatter facility of CERN,[17] Geneva, Switzerland, we use ultra-sensitive Penning-trap techniques to study the fundamental properties of single antiprotons, protons, and hydrogen ions to test the fundamental charge, parity, and time reversal (CPT) invariance. These state-of-the-art tests include the measurement of the antiproton magnetic moment with 1.5 p.p.b. (parts per billion) precision[18] and the comparison of the antiproton-to-proton charge-to-mass ratio with a fractional precision of 16 p.p.t.,[19] constituting the most precise test of CPT invariance in the baryon sector. With this measurement, we also conducted the first differential clock-based test of the weak equivalence principle with antimatter. To perform these single (anti)particle experiments, it is essential to store and non-destructively observe antimatter for many months,[20] which requires vacuum pressures below 10^{-17} mbar, constrained by antiproton/residual-gas annihilation cross sections.[21] The high detection sensitivity of the experiment and the low particle consumption rate mean that only 100 antiprotons need to be transmitted through the window. On the other hand, the vacuum requirements of our non-destructive antimatter experiments are an outstanding challenge.

In this article, we present a solution to this application with the development, design study, and characterization of a vacuum window that is based on aluminized polymer foil. The studied foils have thicknesses between 0.9 and 2.3 μm and can withstand a pressure difference of up to 1300 mbar with a leak rate below 1×10^{-9} mbar l/s at temperatures below 10 K. We first present the technical design of the window together with the experimental setup. This is followed by a general experimental study of the window leak rate for different parameters such as the foil thickness and the open area of the developed window. In this context, we report the first dedicated study of the permeation constant of polymer foils with different aluminum coating thicknesses in room temperature and cryogenic environments and summarize our results of thermal and mechanical endurance and stress tests. Next, we present the first characterization of the degrading properties of pure or aluminized polymer foils of different thicknesses for a 100 keV antiproton beam, essential information for several other experiments in the field. We conclude our work with the successful demonstration of proton trapping for 296 days in a vacuum created by the degrader window.

II. BASE EXPERIMENTAL SETUP

An overview of the BASE experimental setup is shown in Fig. 1. The Penning-trap experiment makes use of a superconducting magnet operated at a magnetic field of $B_0 \approx 1.95$ T with a horizontal bore. The trap itself is operated under cryogenic conditions; the cold temperatures are provided by helium-bath cryostats located on the upstream and downstream sides of the experiment. The upstream side of the apparatus is connected to the AD/ELENA antiproton beamline. Ion-optical elements steer and focus the antiprotons on the entrance flange of the magnet bore and the trap chamber. The outer vacuum in the bore of the magnet, the vacuum crosses that support the cryostats, and the beam tubes form a closed outer

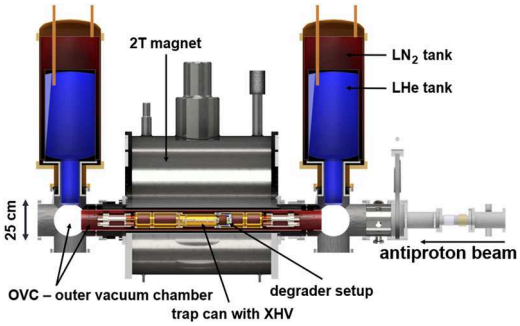

FIG. 1. Cutaway view of the BASE experiment. The Penning-trap electrodes are enclosed inside the trap can, which reaches 10^{-18} mbar (XHV). It is placed inside the 2 T superconducting magnet and outer vacuum chamber (OVC), which allows us to cool the experiment using liquid nitrogen (LN_2) and liquid helium (LHe). The cryogenic window (degrader setup) presented in this paper is an interface piece that closes the vacuum of the trap can while allowing the transmission of 100 keV antiprotons to the trap.

vacuum chamber (OVC), in which pressures of $<10^{-7}$ mbar are achieved. In the homogeneous center of the magnet, the trap is located, enclosed by the *trap can*, which is a cylindrical chamber with a volume of about 1.5 l made out of high purity (OFHC) copper. To separate the trap chamber vacuum from the insulation vacuum, the trap can is closed with custom-made flanges, a feedthrough flange (*pinbase*) on the downstream side, and a *degrader flange* on the upstream side. On this upstream degrader flange, described in detail later in the text, a hard-soldered high-purity annealed copper pinch-off tube and the vacuum window are located.

The extreme high vacuum (XHV) inside the trap can be achieved in several steps. First, the trap system is mounted in the trap can and closed by the respective flanges. Afterward, while baking to about 340 K, the closed trap can is pumped via the pinch-off tube to a level of 10^{-7} mbar. Having reached this pressure, the pinch-off tube is sealed by cold-welding it with an appropriate tool. Only after this step the trap is in the OVC, which means that the degrader window has to hold atmospheric pressure. To reach the 10^{-17} mbar pressure required to store antiprotons for at least a year, we accept a maximum leak rate through the window of $\approx 1 \times 10^{-8}$ mbar l/s for an atmospheric pressure difference at room temperature. In this case, when cooled to cryogenic temperatures, the adsorption of the residual gas on the walls of the trap can and the trap electrodes (cryopumping) is sufficient to reach the XHV pressures required in our experiments.

The 100 keV energy of the antiproton beam provided by CERN's newly implemented ELENA decelerator[22] puts another demanding limit on the vacuum window. The degrader must decrease the energy of the antiproton beam from 100 keV to about 1 to 5 keV to allow particles to be captured efficiently in the Penning trap. This necessitates a polymer foil of thickness below 2 μm. Simultaneously meeting the demanding requirements of low leak rate, efficient antiproton degrading at acceptable particle flux, robustness, reproducibility, and high reliability over months of particle impact and cryogenic operation is a significant technological challenge and the motivation for this work.

III. DEGRADER WINDOW

The main parameter characterizing the vacuum, diffusion, and permeation properties of a foil of thickness d and open surface A is its leak rate for a given pressure difference Δp equal to

$$L_{\text{foil}}(A, d, \Delta p) = K_{\text{foil}} \times \frac{A}{d} \times \Delta p.$$

Here, K_{foil} is the permeation constant[23,24] of the foil. The vacuum window described in this article is based on biaxially oriented polyethylene terephthalate, $H_8C_{10}O_4$, commonly known as Mylar® (DuPont Teijin Films trademark). This material has a permeation constant at the level of 10^{-12} m^2/s measured at room temperature, and its high mechanical and thermal endurance properties were already reported earlier.[23,25]

A detailed schematic that illustrates the technical implementation of the degrader window is shown in Fig. 2. The critical vacuum interface, the *degrader flange*, closes the trap can and separates the XHV of the trap can from the outer isolation vacuum chamber of the experiment. The flange is also the support structure of the developed semi-transparent vacuum window. Moreover, the pinch-off tube for pre-pumping the trap-can vacuum is hard-soldered into this flange.

The window itself is based on *aluminized Mylar foil* glued with a thin layer of Apiezon® N grease[26] on the mesh-like *stamp* with several transmission channels that define the final geometrical particle beam acceptance. Both pieces are attached to the degrader flange by a *clamp*, which ensures even pressure distribution over the used seals. As both Mylar and aluminum are not self-sealing, the main seal is achieved using indium placed inside the grooves of the degrader flange, which is squeezed by the stamp with the clamp. The double indium seal is used for additional safety. To protect the foil from being torn by the ductile indium seal, the outer part of the foil is covered with a polished Kapton® ring. The sizes of all elements were optimized to fit into the magnet bore of the BASE apparatus.[5] The effective transparent surface of the window is defined by the holes in the stamp, which form transmission channels for the particles [see Fig. 2(b)]. To reach the highest possible beam transmission, we performed different systematic studies of various geometries described later in the text. The final configuration used for the experiments with the antiproton beam has a stamp with seven holes of diameter 1 mm each, placed in the center and the corners of a regular hexagon with a side length of 1.5 mm. This configuration gives 17% geometrical acceptance for the ELENA antiproton beam, which, in a plane perpendicular to the beam direction, is characterized by a full width at half maximum of about 5 mm. Based on empirical studies, a mechanically polished fillet radius of at least 0.1 mm for each hole reproducibly prevents rupture and damage to the foil. Equally important is to polish each part of the seal. This creates uniform surfaces and prevents surface leaks. The stamp implemented into the experiment has a surface roughness[27] of arithmetic mean deviation $R_a = 0.42\ \mu$m, maximum height $R_z = 2.17\ \mu$m, maximum profile peak height $R_p = 1.16\ \mu$m, mean spacing of profile irregularities $S_m = 31.12\ \mu$m, reduced peak height $R_{pk} = 0.25\ \mu$m, and reduced valley height $R_{vk} = 0.32\ \mu$m.

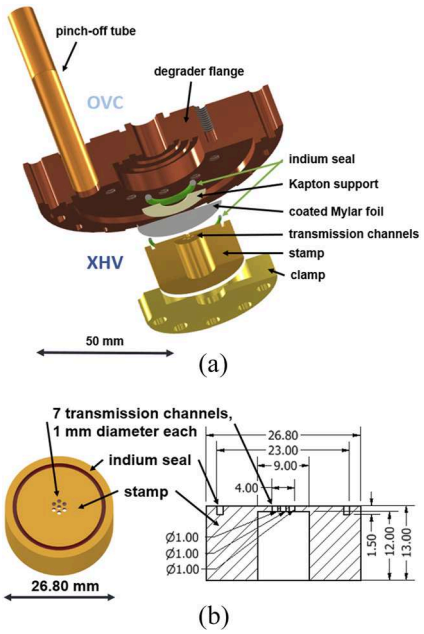

FIG. 2. (a) Detailed scheme of the cryogenic, vacuum-tight degrading window that separates the XHV (10^{-18} mbar) of the experimental chamber from the surrounding OVC vacuum (10^{-7} mbar). The main part is the degrader flange with a soldered pinch-off tube that closes the trap can. The seal consists of a tightly pressed indium ring that is placed between the flange and Kapton ring supporting the coated Mylar foil on a stamp, which is kept in place using a clamp. (b) Zoom on the stamp geometry and the transmission channels. On the left, an overview drawing and, on the right, the cross-sectional view with dimensions in mm are shown.

IV. PERMEATION CONSTANT MEASUREMENTS

During the window development phase, we performed different measurements of the helium leak rate through various foils, both at room- and cryogenic temperatures, using the experimental setup shown in Fig. 3. The setup consists of a degrader chamber that can be cooled to $T < 10$ K using a Sumitomo RDK-408D2 cryocooler. All elements of the degrader chamber connected to the second cooling stage are made of oxygen-free high thermal conductivity (OFHC) copper for the best possible thermal conductivity and nonmagnetic properties. Using Swagelok stainless steel connections, one side of the degrader chamber is pumped using the turbomolecular pump built into a Leybold Phoenix L300i leak detector, which allows us to measure the helium leak rate through the designed window down to the level of 1×10^{-12} mbar l/s. The other side of the degrader chamber is connected to the helium supply, which provides up to 2 bars of He pressure. We use He as a test gas as it has the highest permeation constant. Before inserting gas, the chamber is first pumped to a pressure of around 1×10^{-1} mbar.

In this section, we characterize the leak rate through different foils. Unless otherwise noted, the measurement was performed for 1 bar of helium pressure applied to the inlet, measured using a Baratron 120AA from MKS Instruments. To establish that any measured leaks were due to permeation through the foils rather than leaks through the indium seals, we performed different leak rate measurements with a 200 μm thin aluminum foil instead of the Mylar foil. Both at 300 K and at cryogenic temperatures, these measurements reached the background sensitivity of the leak detector, from which we conclude that the measured leak rate corresponds to

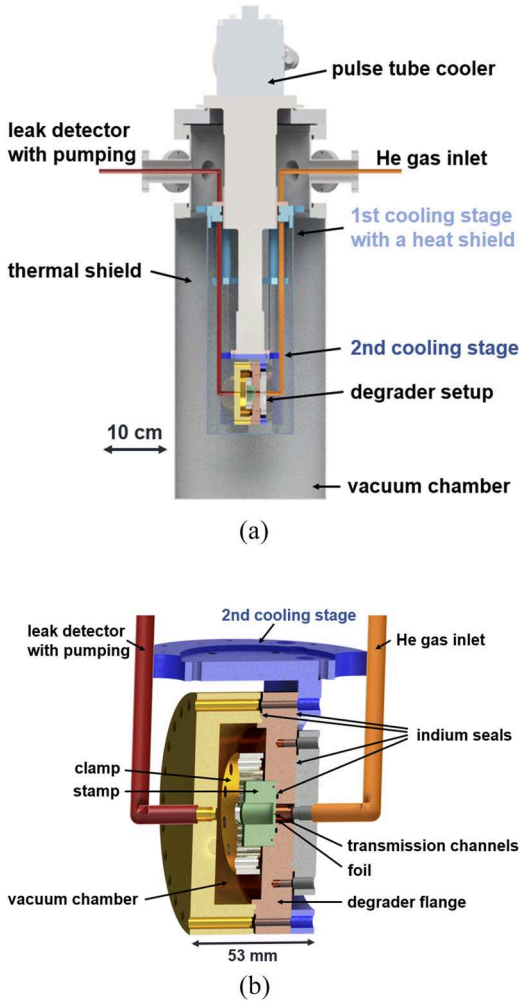

FIG. 3. Schemes of the setup used to test the cryogenic window at temperatures down to 2.7 K. (a) A full scheme of the setup based on the Sumitomo RDK-408D2 cryocooler with two cooling stages. The helium gas is supplied to the test chamber via an 8 mm diameter tube from the gas bottle. The pressure applied to the system is controlled in multiple stages using a pressure reducer and helium preparation vacuum chambers. The other side of the test chamber is pumped via a leak detector, which allows a measurement of the flow of the helium gas through the tested cryogenic window. (b) Zoom of the second (2.7 K) cooling stage where the chamber with the degrader is placed.

the permeation through the degrader foil itself. This was also confirmed by executing reproducibility tests using the same Mylar foil in technically identical assemblies but in different characterization runs.

A. Tested materials

We tested a variety of pure Mylar foils with thicknesses between $d = 0.5$ μm and $d = 2.5$ μm, and Mylar foils metallized on one or both sides with varying thicknesses of the aluminum layers. The aluminum layer was coated using two methods, either magnetron sputtering[28] or the evaporation of metal in a vacuum.[29] Magnetron sputtering allows the production of aluminum coating thicknesses between 25 and 200 nm, as stated by the producer of the foil and confirmed by measurements using a precise weighting scale. We obtained Al-coating thicknesses of 30 and 80 nm for the evaporation-coated foils, as these were commercially available thicknesses.

B. Impact of the aluminum coating

Permeation through biaxially oriented polymer foils can be suppressed by metallizing the polymer film. The coating closes the porous polymer structure and suppresses atomic and molecular diffusion. To investigate this effect quantitatively, we study the leak rate as a function of coated Al thickness λ. As a base material, 900 nm Mylar foil coated on both sides was used. Four different magnetron sputtered foils with coating thicknesses between 25 and 200 nm were tested, and the measured permeation constants are plotted in Fig. 4.

Using the experimental setup described earlier and mounting the foils with the seven-hole support stamp to close the window, the leak rate of each of the foils was measured at 300 K. In the experiments, the system was first pumped for 60 min, then the high

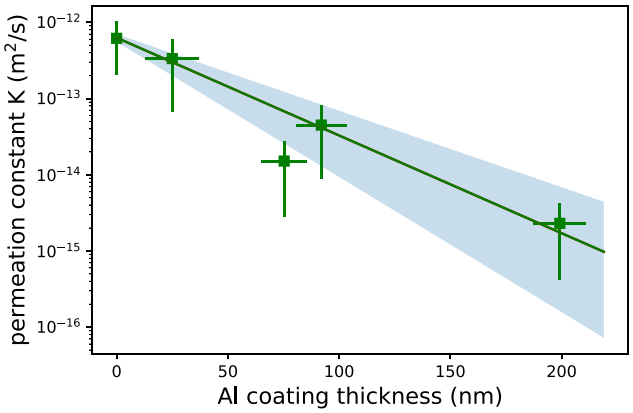

FIG. 4. Permeation constant for 900 nm thick Mylar foil as a function of the aluminum coating thickness added on both sides together with a shaded $\pm 2\sigma$ confidence interval of the fitted exponential function. Uncertainties are dominated by the measurement of the foil thickness. Each leak measurement is an average of over 60 min of data (3600 points), collected 60 min after the start of pumping. These measurements were performed with a stamp with seven 1-mm-diameter holes. The point at 0 nm aluminum thickness is a reference point to a pure Mylar foil measured with a stamp with one 1.2 mm diameter hole. The measurement was performed at room temperature.

TABLE I. Permeation constants of Mylar foils without, with one, or both sides aluminized (layer thickness 80 nm). The foils were metallized by evaporation. Measured at room temperature with one 1.2 mm diameter transmission channel.

Foil	K_{foil} (m^2/s)	Leak rate (mbar l/s)
2.5 μm Mylar	1×10^{-12}	5×10^{-7}
2 μm Mylar + 80 nm Al	4×10^{-14}	2.2×10^{-8}
2 μm Mylar + 80 nm Al on each side	4.6×10^{-15}	1.9×10^{-9}

TABLE II. Measured leak rate through the 2160 nm aluminized Mylar foil as a function of a single hole diameter.

Hole diameter (mm)	Permeation constant K (m^2/s)
1.0	$3.4(1.3) \times 10^{-15}$
1.2	$4.6(1.5) \times 10^{-15}$
1.5	$3.7(1.1) \times 10^{-15}$

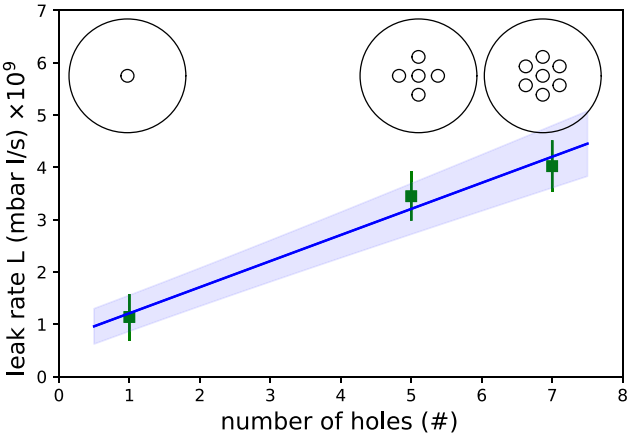

FIG. 5. Measured leak rate through the 2160 nm aluminized Mylar as a function of the number of 1-mm-diameter holes with a fitted straight line (blue) together with a shaded 2σ confidence interval.

pressure side of the window was vented with 1 bar of helium, and the leak rate was recorded for 60 min with a 1 s sampling rate. The mean results of this characterization campaign are shown in Fig. 4. The quoted uncertainties reflect the fluctuations of the measurements, and the shaded area covers the $\pm 2\sigma$ confidence interval of a fit with an exponential function of type $\propto \exp(-\lambda/\lambda_0)$ with the effective permeation reaching $\lambda_0 = 33.9 \pm 4.7$ nm. The point at zero aluminum thickness is a reference point using uncoated Mylar foil. We observe that the change in the thickness of the aluminum layer from 25 to 200 nm decreases the leak rate by two orders of magnitude. We note that the mechanical properties of the foil with 200 nm Al-coating were dominated by the properties of the fragile aluminum-layer, which is prone to cracking when stretched.

Results of less systematic but similar experiments with foils produced by vapor metallization are summarized in Table I showing qualitatively similar behavior for these foils.

C. Optimization of the stamp geometry

Aluminized Mylar foil in the thickness range investigated here is very sensitive to stretching and sharp edges. That is why a circular shape of the window is used so that the forces introduced by stretching and cooling are uniformly distributed over the foil surface. To optimize the size of the window, we studied the leak rate through a 2 μm Mylar foil coated on both sides with 80 nm aluminum (later referred to as 2160 nm aluminized Mylar foil) while supporting it with a stamp with a single central hole. In these experiments, we varied the hole diameter and determined the permeation constant of each assembly. The results as a function of the single hole diameter are presented in Table II. In the range between 1 and 1.5 mm of hole diameter, we measure permeation constants that are similar within the measurement uncertainties. At 2 mm in diameter, the permeation constant of the foil was observed to continuously increase due to developing damage to the foil structure caused by stretching. For our geometries, this behavior was reproducibly observed in repetitive experiments. On the other hand, up to a 1.5 mm diameter hole, the leak rate was constant even after many days of data sampling.

Selecting a hole diameter of 1 mm, we have investigated the leak rate as a function of the number of holes distributed over the surface of the degrader window. The results of this study are shown in Fig. 5.

Up to seven holes, we see a linear scaling of the leak rate as a function of the transparent surface area, indicating no inelastic damage while pumping the foil. For an even higher number of holes and the selected geometries, we observed irreversible damage. In the final design, we chose to use seven holes, as the transparency of the window with the centered hexagonal hole distribution with respect to the ELENA beam is 17%.

V. CRYOGENIC CHARACTERIZATION

In the BASE experiment, the described window will be operated at a temperature of about 4.5 K to separate the XHV of the trap can from the isolation vacuum of the experiment. That is why, for foils of thicknesses 2160, 1960, and 1760 nm, all coated on both sides with a vaporized Al-layer of 30 nm thickness, we performed various endurance tests. Within this testing campaign, we exposed the foil assemblies to mechanical stress under room temperature and cryogenic conditions while measuring the leak rate with the cryogenic

TABLE III. The average leak rate measured for different foils at both room and cryogenic (below 10 K) temperatures. Each value is an average of 9000 measurement points, covering a time interval of at least 1 h. The leak was measured under 1200 mbar helium pressure at room temperature with a Baratron.

Foil	Average leak rate at 293 K (mbar l/s)	Average leak rate at 6–10 K (mbar l/s)
2 μm Mylar + 80 nm Al on both sides	$5.49(0.02) \times 10^{-9}$	$2.49(0.09) \times 10^{-11}$
1.9 μm Mylar + 30 nm Al on both sides	$1.467(0.004) \times 10^{-8}$	$4.8(0.6) \times 10^{-10}$
1.7 μm Mylar + 30 nm Al on both sides	$1.46(0.07) \times 10^{-8}$	$6.57(0.05) \times 10^{-10}$

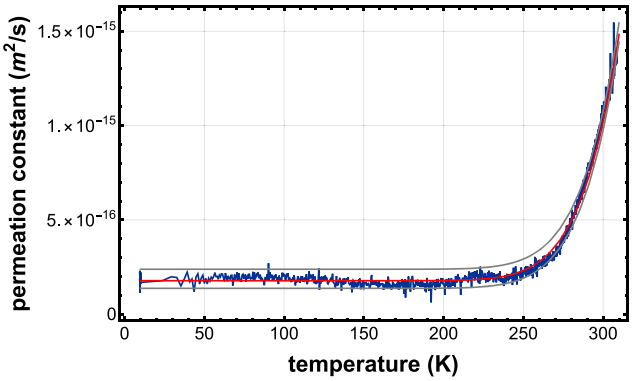

FIG. 6. Leak rate through a 1960 nm thick foil as a function of its temperature. The data were treated with a median filter with a time step of 19.8 s.

test-setup described earlier (see Fig. 3). Additionally, using a similar experimental setup, we expose the windows to thermal shocks by pouring a direct stream of liquid nitrogen onto the foils while continuously measuring the leak rate.

The summary of the measured average leak rate for the three tested foils at room temperature and at cryogenic temperatures below 10 K is presented in Table III. We observe that the leak rates at $T = 300$ K and $T < 10$ K differ by about one order of magnitude.

The temperature dependence of the permeation constant through polymers can be empirically described by the van Hoff–Arrhenius relation,[30] where the dependence is parameterized by the effective sorption, desorption, and diffusion dynamics that obey effective thermodynamic scaling laws $\propto \exp(-\Lambda_p/T)$. The leak rate as a function of temperature was measured while the apparatus was warming up; exemplary data are shown in Fig. 6. Interestingly, the leak rate as a function of temperature reproducibly shows for all the tested foils a rapid decrease in the temperature range between 300 and 250 K, then staying constant down to $T < 10$ K.

For smooth long-term experimental operation in a cryogenic precision experiment, long-term stability and resilience with respect to repetitive cooling/warming cycles and stretching due to a change in pressure difference experienced by the foil are essential. To study the long-term stability of the degrader window, we kept the 2160 nm thick foil at 10 K temperature under a stationary helium pressure of 1200 mbar for 25 days. Figure 7(a) shows a 68 h long interval

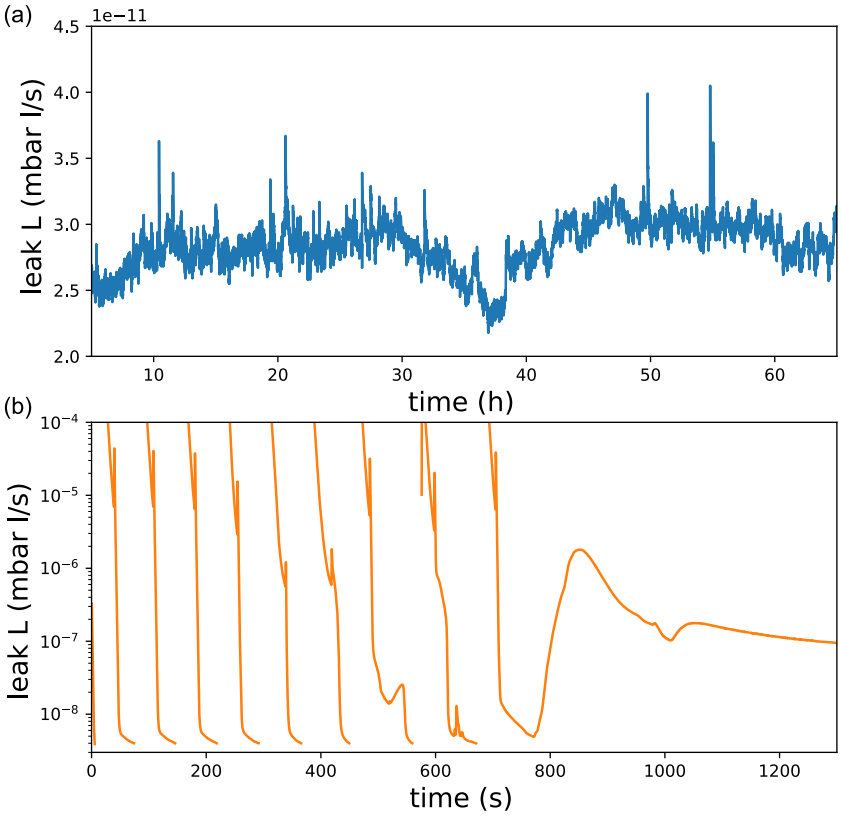

FIG. 7. Cryogenic endurance tests with a 2160 nm thick foil. (a) A 68 h long exemplary interval of the leak rate measurement at 10 K. The full experiment lasted for 25 days. (b) Leak rate as a function of time while performing a cryogenic endurance test carried out at 77 K with liquid nitrogen. The foil was continuously pumped and re-pressurized. The leak rate was limited by the thermal expansion of the support vacuum chamber; for further details, refer to the text. The test was performed with a single hole with a diameter of 1.2 mm as the transmission channel.

of the measured leak rate, representative of the stability that was observed over the entire 25 days. The 25% baseline drift around the level of 2×10^{-11} mbar l/s is correlated with laboratory temperature changes; the fluctuation spikes with amplitudes at the 10^{-10} mbar l/s level are likely induced by vibration and out-gassing of micro-enclosures in the beam tubes. Before and after this measurement, the foil was thermally cycled several times and exposed to ten sequences of pressure changes between 0.1 and 1200 mbar at ramp times between 10 and 100 s. Eventually, the system was re-cooled and the leak rate was measured again. During all these stress tests, the load amplitude and time constants were much higher than the expected changes during the experiment operation, but we did not detect an increase in the measured leak rate within the 5% resolution limit of the measurement.

Finally, while measuring the leak rate, we exposed the window to thermal shocks by sinking it into liquid nitrogen (LN_2), corresponding to quasi-instantaneous temperature changes of 220 K per cycle. Additionally, we performed stretching tests at LN_2 temperature by venting the pumping system and the leak detector, thus changing the pressure difference experienced by the foil. In these tests, we pumped the system until the measured leak was smaller than 4×10^{-9} mbar l/s, then vented the system to 1 bar of He pressure and pumped again afterward. The result of this test is shown in Fig. 7(b). Eight full pumping cycles were successful. The reduced performance after the ninth cycle was found to be caused by a cryo-leak in the supporting vacuum chamber, not by degradation of the window.

In summary, all three foils, 2160, 1960, and 1760 nm, were cooled at least twice, with multiple foil stretching tests performed by varying the helium pressure in the system both at room and cryogenic temperatures. Within these measurements, we were not able to resolve any indication of degradation or mechanical fatigue behavior of the foil. The window also withstands long term operation and cryogenic temperature and survived endurance, pressure, and thermal shocks that are partly by three orders of magnitude more extreme than expected under the final experimental conditions. Therefore, all three foils meet the requirements to be implemented in the experiment.

VI. ANTIPROTON DECELERATION

The vacuum window presented earlier has the crucial role of being a degrader for the 100 keV antiproton beam delivered by CERN's ELENA decelerator. In this section, we present the results of the characterization of the degrading properties of Mylar foils of different thicknesses, which allows matching the thickness of the window to the initial and required final energy of antiprotons.

A. Theoretical estimation of the required foil thickness

At the time when the window was designed, there was a lack of experimental data and models for the stopping power of antiprotons in Mylar in the energy range between 1 and 100 keV. To approximately estimate the range of thicknesses for the degrading Mylar foil, we developed an effective guiding model based on the measured stopping power data of antiprotons in carbon[31] and the available stopping power data of protons in different materials. The data for protons were taken from the scientific community code SRIM.[32] According to Bragg's rule,[33] in first order, the stopping power $S(E)$ in a compound material can be estimated as a linear combination of the stopping powers of its components. In the case of Mylar $H_8C_{10}O_4$, this results in

$$S(E)_{\mathrm{Mylar/p}} = \frac{8}{22} \times S(E)_{\mathrm{H/p}} + \frac{10}{22} \times S(E)_{\mathrm{C/p}} + \frac{4}{22} \times S(E)_{\mathrm{O/p}},$$

where $S(E)_{\mathrm{H,C,O/p}}$ are the stopping powers of protons in hydrogen, carbon, and oxygen, respectively. In more recent calculations that account for atomic bonding effects, Bragg's formula is multiplied by the compound correction, which is given for Mylar as 0.9570.[32] To a good approximation, it is expected that the stopping power for antiprotons in Mylar can be described using the same formula but using stopping powers for antiprotons. To compensate for the lack of available $S(E)_{\bar{\mathrm{p}}}$ data for antiprotons, which was in the expected energy range only measured for carbon or aluminum,[31] we describe $S(E)_{Mylar/\bar{\mathrm{p}}}$ as $S(E)_{\mathrm{C}/\bar{\mathrm{p}}}$ multiplied by a scaling factor λ,

$$S(E)_{\mathrm{Mylar}/\bar{\mathrm{p}}} = \lambda \times S(E)_{\mathrm{C}/\bar{\mathrm{p}}},$$

where $S(E)_{\mathrm{C}/\bar{\mathrm{p}}}$ is an extrapolated fit to the data from Ref. 31. To obtain a realistic estimate of the value of the effective parameter λ, we use data for the stopping power of protons in Mylar and carbon and calculate λ as

$$\lambda = \frac{S(E)_{\mathrm{Mylar/p}}}{S(E)_{\mathrm{C/p}}} = 0.620 \pm 0.002,$$

for the energy range between 1 and 100 keV. We show below that this effective approach is within the measurement uncertainties in agreement with our measurements.

Recently, the first experimental data for the stopping power of low-energy antiprotons for 1800 nm Mylar foil coated with two 25 nm thick silver layers were published in Ref. 34. In the same

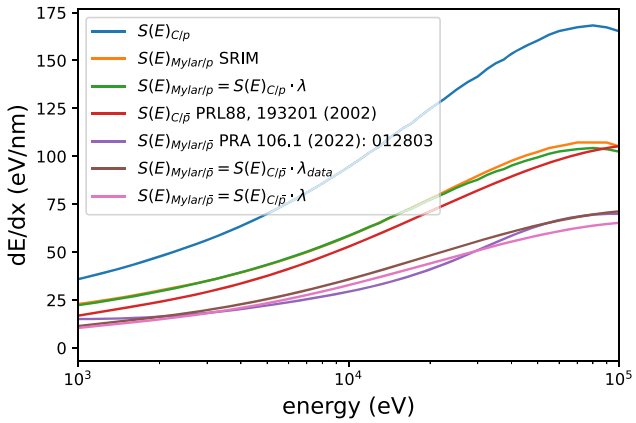

FIG. 8. Stopping power values for protons p or antiprotons $\bar{\mathrm{p}}$, for carbon—$S(E)_{\mathrm{C/p}(\bar{\mathrm{p}})}$; Mylar (from SRIM)—$S(E)_{Mylar/\mathrm{p}}$; Mylar (from Ref. 34)—$S(E)_{Mylar/\bar{\mathrm{p}}}$; Mylar according to the model described in the text—$S(E)_{Mylar/\bar{\mathrm{p}}} \cdot \lambda$; Mylar according to the model described in the text with parameter λ fitted to the data—$S(E)_{Mylar/\bar{\mathrm{p}}} \cdot \lambda_{data}$.

paper, the authors provide calculations of the electronic and nuclear stopping power of antiprotons in Mylar using a molecular dynamics approach. The main advantage of these results is that for the first time, nuclear scattering effects for antiprotons were included in the calculation, which significantly enlarged the values of the nuclear stopping power around 1 keV energies. The comparison of this refined model to our measurements is also shown in Sec. VI B. Figure 8 compares the stopping power curves in an energy range between 1 and 100 keV, which were described in this section, with a stopping power curve obtained from the measurements described in the following text.

B. Degrading properties of the Mylar foil

Using CERN's 100 keV ELENA beam, we tested the degrading properties of different thicknesses of Mylar or aluminized Mylar foils to explicitly measure the optimum foil thickness for antiproton injection into our system. For this, we performed a time-of-flight measurement of particles transmitted through the degrader within a 6° angle, and the relevant data were recorded with a set of scintillation counters placed along the antiproton transfer line.[5] The transmitted particles annihilated at least 65 cm behind the degrader, which enables us to distinguish them from particles annihilating inside the degrader and allows for an estimation of the energy of the slowed antiprotons. For a better understanding of the transmitted signal, we used a movable target whose perpendicular position with respect to the beam axis was adjusted using a piezo-driven linear slip-stick stage, specified for operation in high magnetic fields and under ultra-high vacuum conditions.[35] The target had three positions: open—in which the beam transmits undisturbed; block—in which the entire beam annihilates on the target; and foil—where the beam transmits through a 9 mm diameter aperture covered by the foil under test. This combination of measurements allows us to distinguish different backgrounds originating from beam annihilation in different parts of the system. Tests were performed for four different foils: 900 nm thick pure Mylar, 900 nm thick Mylar with two 100 nm thick layers of Al, 1400, and 1700 nm, both foils covered with two Al-layers of 30 nm thickness.

The measured energy of the transmitted beam as a function of the foil thickness is shown in Fig. 9. We determine the mean energy based on the simulated pulse-shapes using SRIM[32] and obtain the mean energy by deconvolving the data with simulation-based effective profiles that reproduce the data within the residuals of the background noise of the detector. Small deviations from the expected profiles are attributed to annihilations on obstacles along the beamline of the cryogenic Penning trap experiment. A detailed study of the consistency of model assumptions and measured profiles would require a redesign of parts of the cryogenic Penning trap experiment and is beyond the scope of this article. The data are compared to simple simulation results in which particles go straight through the pure Mylar foil, assuming two different models for the stopping power of Mylar—model A described in Sec. VI A and model B taken from Ref. 34. Taking into account only particles that go straight through a Mylar foil is a correct approximation, as the measured delayed signal originates from particles that are transmitted through the foil with an angular transverse momentum spread smaller than 6°. In the simulations, we are neglecting the difference between the stopping power of aluminum and Mylar, as the thickness of aluminum is relatively small compared to the thickness of Mylar, and the measured stopping power of aluminum[31] is only up to 30% larger than the estimated stopping power for Mylar. The new calculations presented in Ref. 34 confirm this assumption. Our measurements and both models are in qualitative agreement. Based on the fit to the data, we extracted the parameter $\lambda_{data} = 0.677 \pm 0.066$, which is in agreement with our theoretical prediction and can be used to simulate in a simple way the behavior of antiprotons going through Mylar.

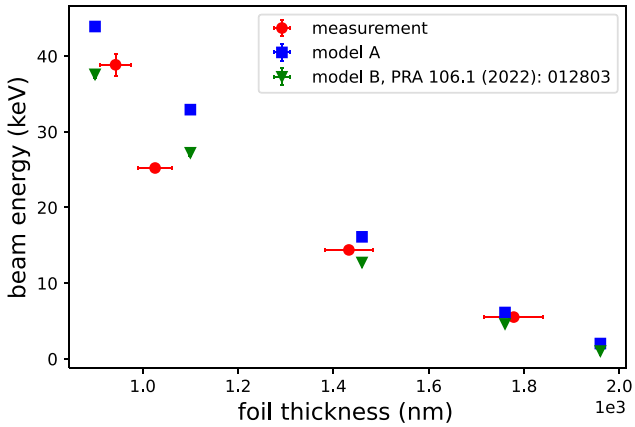

FIG. 9. Measured energy of the transmitted beam as a function of the foil thickness (red round points) compared to the simple phenomenological model presented in Sec. VI A based on measured data of the stopping power of antiprotons in carbon[31] (blue squares) and the model presented in Ref. 34 (green triangles).

For efficient trapping, BASE can accept particles between 1 and 5 keV energy after the degrading stage. That is why in the final assembly we decided to use foils of thickness 1760 and 1960 nm, which should allow us to transmit up to 2.5% of the injected 100 keV antiprotons.

VII. INTEGRATION INTO THE BASE EXPERIMENT

The implementation of the designed foil system into the BASE setup, as a degrader for the antiproton beam and as an XHV window to close the trap can, is shown in Fig. 10. While operating the experiment, all components shown in the drawing are at $T < 5.2$ K. The interface between the trap and the degrader flange is called a degrader chamber, in which a copper foam absorber is placed to increase the adsorption surface for cryopumping. The copper foam increases the cryogenic metal surface in the trap by a factor of 2.5. The distance between the degrader window and the center of the most upstream trap, the reservoir or catching trap, is ≈11.6 cm. The entire volume between the degrader window and trap center is placed in a background magnetic field >1.5 T. We note that upstream from the reservoir/catching trap, a repeller electrode is placed. Antiproton catching relies on electron cooling. Before antiprotons are injected, a cloud of electrons is loaded into the catching trap, which rapidly cools to thermal background temperatures through the emission of cyclotron radiation. Antiprotons injected into high-density electrons are sympathetically cooled by the

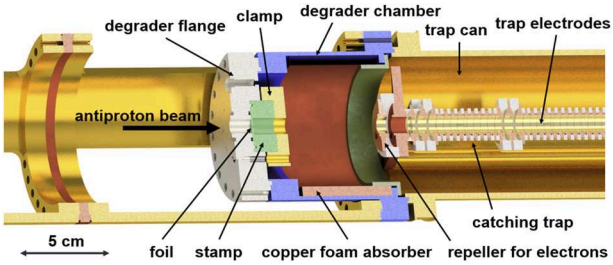

FIG. 10. Scheme of the new, vacuum-tight, micrometer-thick degrader window implemented in the BASE experiment.

scattering on- and cyclotron radiation of electrons. To protect the degrader foil from the 40 to 80 eV electron beam, which is typically operated at currents of 20 to 200 nA, the repeller electrode is biased to twice the kinetic energy of the electron beam.

A. Trapped charged particles

For the commissioning of the experiment, we load a cloud of protons using the molecular hydrogen dissociation mechanism of the electron beam. With the designed vacuum system closed with the 1960 nm foil, no particle loss or decreased performance of the experiment was observed throughout a continuous observation time lasting from the 10th of October 2021 to the 1st of August 2022, i.e., for 295 days. We also observed that the implemented vacuum window robustly survived several experiment cooling cycles between 300 and 5 K at temperature ramping rates of 24 h per cycle for both warm-up and cool-down, an important feature for the practical operation of the experiment. After operating the system under cryogenic and high vacuum conditions for 295 days, the experiment was warmed up for technical radiofrequency maintenance, and the degrader window was extracted and investigated again in the experimental test setup. In these studies, we measured the leak through the foil at 8.5×10^{-8} mbar l/s. Currently, it is not possible to conclude whether the slightly increased leak rate from $1.46(0.07) \times 10^{-8}$ mbar l/s (Table III) is related to mechanical fatigue or to overpressurization in the reassembled test setup. To further optimize antiproton catching in BASE, the next run was operated with the 1760 nm foil. Up to the date of writing this article (216 days), no decrease in the experiment's performance due to increased pressure was observed. The lowest pressure limit that was estimated based on explicit measurements comes from the observation of quantum heating rates of a single trapped proton in the strong magnetic bottle of the analysis trap of the experiment.[5] By initially cooling the magnetron mode to particle energies $<0.6(6)\,\mu$eV, performing experimental campaigns for typically 72 h, and recooling the magnetron mode afterward, within the uncertainties of the experiment, we did not resolve any statistically significant heating mechanism. This constrains the collision-related cooling time constant to levels $>5 \times 10^5$ s and gives, combined with the thermodynamic treatment reported in Ref. 36, a pressure estimate of $p < 10^{-15}$ mbar. More accurate pressure estimates will become possible with antiproton lifetime measurements, which will be one of the primary objectives of the next antiproton run.

VIII. CONCLUSIONS

We presented the development and detailed characterization of a micrometer thick cryogenic vacuum window based on aluminized Mylar in a wide 900 to 2160 nm thickness range that sustains a pressure difference of up to 1300 mbar.

Various optimization and endurance tests indicate that the window properties do not degrade after one year of operation at 4 K temperature. Using this window, we managed to reach a leak rate smaller than $6.57 \pm 0.05 \times 10^{-10}$ mbar l/s measured at a cryogenic temperature at 1 bar helium pressure with a foil of only 1760 nm thickness. According to the measured degrading properties of the Mylar foil, the designed system enables us to transport a low energy antiproton beam provided by the AD/ELENA facility at CERN to the inside of the apparatus. For 1760 nm foil and 5 kV potential on the trapping electrodes, we expect to be able to trap up to 2.5% of the 100 keV antiproton beam. Given all the presented results, we have shown that the developed system meets the requirements for lossless antiproton trapping for at least 12 months.

ACKNOWLEDGMENTS

We acknowledge financial support by RIKEN, the Max-Planck Society, CERN, the European Union (FunI-832848, STEP-852818), CRC 1227 "DQ-mat" (DFG 274200144), the Cluster of Excellence "Quantum Frontiers" (DFG 390837967), the Wolfgang Gentner Program (Grant No. 13E18CHA), IMPRS-QD, and the Helmholtz-Gemeinschaft. This work was supported by the Max-Planck, RIKEN, PTB-Center for Time, Constants, and Fundamental Symmetries (C-TCFS).

AUTHOR DECLARATIONS

Conflict of Interest

The authors have no conflicts to disclose.

Author Contributions

B. M. Latacz: Conceptualization (lead); Data curation (lead); Formal analysis (lead); Investigation (lead); Methodology (lead); Project administration (lead); Software (lead); Validation (lead); Visualization (lead); Writing – original draft (lead); Writing – review & editing (lead). **B. P. Arndt**: Writing – review & editing (supporting). **J. A. Devlin**: Investigation (supporting); Methodology (supporting); Software (supporting); Validation (supporting); Writing – original draft (supporting); Writing – review & editing (supporting). **S. R. Erlewein**: Writing – review & editing (supporting). **M. Fleck**: Data curation (supporting); Writing – review & editing (supporting). **J. I. Jäger**: Writing – review & editing (supporting). **P. Micke**: Data curation (supporting); Writing – review & editing (supporting). **G. Umbrazunas**: Data curation (supporting); Writing – review & editing (supporting). **E. Wursten**: Writing – review & editing (supporting). **F. Abbass**: Writing – review & editing (supporting). **D. Schweitzer**: Writing – review & editing (supporting). **M. Wiesinger**: Writing – review & editing (supporting). **C. Will**: Writing – review & editing (supporting). **H. Yildiz**: Writing – review & editing (supporting). **K. Blaum**: Funding acquisition (equal); Resources (equal); Writing – review & editing (supporting).

Y. Matsuda: Writing – review & editing (supporting). **A. Mooser**: Writing – review & editing (supporting). **C. Ospelkaus**: Writing – review & editing (supporting). **C. Smorra**: Software (supporting); Validation (supporting); Writing – review & editing (supporting). **A. Sótér**: Writing – review & editing (supporting). **W. Quint**: Writing – review & editing (supporting). **J. Walz**: Writing – review & editing (supporting). **Y. Yamazaki**: Writing – review & editing (supporting). **S. Ulmer**: Conceptualization (supporting); Data curation (supporting); Formal analysis (supporting); Funding acquisition (lead); Investigation (supporting); Methodology (supporting); Project administration (lead); Resources (lead); Software (supporting); Supervision (lead); Validation (supporting); Visualization (supporting); Writing – original draft (supporting); Writing – review & editing (equal).

DATA AVAILABILITY

The data that support the findings of this study are available from the corresponding author upon reasonable request.

REFERENCES

[1] A. Sótér, H. Aghai-Khozani, D. Barna, A. Dax, L. Venturelli, and M. Hori, "High-resolution laser resonances of antiprotonic helium in superfluid ^{4}He," Nature **603**, 411–415 (2022).

[2] T. Tajima and J. M. Dawson, "Laser electron accelerator," Phys. Rev. Lett. **43**, 267 (1979).

[3] P. Chen, J. Dawson, R. W. Huff, and T. Katsouleas, "Acceleration of electrons by the interaction of a bunched electron beam with a plasma [Phys. Rev. Lett. 54, 693 (1985)]," Phys. Rev. Lett. **55**, 1537 (1985).

[4] A. Aschikhin, C. Behrens, S. Bohlen, J. Dale, N. Delbos, L. di Lucchio, E. Elsen, J.-H. Erbe, M. Felber, B. Foster, L. Goldberg, J. Grebenyuk, J.-N. Gruse, B. Hidding, Z. Hu, S. Karstensen, A. Knetsch, O. Kononenko, V. Libov, K. Ludwig, A. Maier, A. Martinez de la Ossa, T. Mehrling, C. Palmer, F. Pannek, L. Schaper, H. Schlarb, B. Schmidt, S. Schreiber, J.-P. Schwinkendorf, H. Steel, M. Streeter, G. Tauscher, V. Wacker, S. Weichert, S. Wunderlich, J. Zemella, and J. Osterhoff, "The FLASHforward facility at DESY," Nucl. Instrum. Methods Phys. Res., Sect. A **806**, 175–183 (2016).

[5] C. Smorra, K. Blaum, L. Bojtar, M. Borchert, K. Franke, T. Higuchi, N. Leefer, H. Nagahama, Y. Matsuda, A. Mooser, M. Niemann, C. Ospelkaus, W. Quint, G. Schneider, S. Sellner, T. Tanaka, S. Van Gorp, J. Walz, Y. Yamazaki, and S. Ulmer, "BASE—The baryon antibaryon symmetry experiment," Eur. Phys. J. Spec. Top. **224**, 3055–3108 (2015).

[6] C. Smorra, F. Abbass, M. Bohman, Y. Dutheil, A. Hobl, D. Popper, B. Arndt, B. Bauer, J. Devlin, S. Erlewein *et al.*, "BASE-STEP: A transportable antiproton reservoir for fundamental interaction studies," arXiv:2304.09555 (2023).

[7] G. Gabrielse, N. Bowden, P. Oxley, A. Speck, C. Storry, J. Tan, M. Wessels, D. Grzonka, W. Oelert, G. Schepers, T. Sefzick, J. Walz, H. Pittner, T. Hänsch, and E. Hessels, "Stacking of cold antiprotons," Phys. Lett. B **548**, 140–145 (2002).

[8] N. Kuroda, H. A. Torii, K. Y. Franzen, Z. Wang, S. Yoneda, M. Inoue, M. Hori, B. Juhász, D. Horváth, H. Higaki, A. Mohri, J. Eades, K. Komaki, and Y. Yamazaki, "Confinement of a large number of antiprotons and production of an ultraslow antiproton beam," Phys. Rev. Lett. **94**, 023401 (2005).

[9] C. Amole, G. Andresen, M. Ashkezari, M. Baquero-Ruiz, W. Bertsche, P. Bowe, E. Butler, A. Capra, P. Carpenter, C. Cesar, S. Chapman, M. Charlton, A. Deller, S. Eriksson, J. Escallier, J. Fajans, T. Friesen, M. Fujiwara, D. Gill, A. Gutierrez, J. Hangst, W. Hardy, R. Hayano, M. Hayden, A. Humphries, J. Hurt, R. Hydomako, C. Isaac, M. Jenkins, S. Jonsell, L. Jørgensen, S. Kerrigan, L. Kurchaninov, N. Madsen, A. Marone, J. McKenna, S. Menary, P. Nolan, K. Olchanski, A. Olin, B. Parker, A. Povilus, P. Pusa, F. Robicheaux, E. Sarid, D. Seddon, S. Seif El Nasr, D. Silveira, C. So, J. Storey, R. Thompson, J. Thornhill, D. Wells, D. van der Werf, J. Wurtele, and Y. Yamazaki, "The ALPHA antihydrogen trapping apparatus," Nucl. Instrum. Methods Phys. Res., Sect. A **735**, 319–340 (2014).

[10] A. Gutierrez, M. Ashkezari, M. Baquero-Ruiz, W. Bertsche, C. Burrows, E. Butler *et al.*, "Antiproton cloud compression in the ALPHA apparatus at CERN," Hyperfine Interact. **235**, 21–28 (2015).

[11] P. Scampoli and J. Storey, "The AEgIS experiment at CERN for the measurement of antihydrogen gravity acceleration," Mod. Phys. Lett. A **29**, 1430017 (2014).

[12] A. Kellerbauer, T. Kim, R. Moore, and P. Varfalvy, "Buffer gas cooling of ion beams," Nucl. Instrum. Methods Phys. Res., Sect. A **469**, 276–285 (2001).

[13] C. Droese, S. Eliseev, K. Blaum, M. Block, F. Herfurth, M. Laatiaoui, F. Lautenschläger, E. Minaya Ramirez, L. Schweikhard, V. Simon, and P. Thirolf, "The cryogenic gas stopping cell of SHIPTRAP," Nucl. Instrum. Methods Phys. Res., Sect. B **338**, 126–138 (2014).

[14] M. Ulbricht, "Advanced functional polymer membranes," Polymer **47**, 2217–2262 (2006), single chain polymers.

[15] T. A. Crowley and V. Pizziconi, "Isolation of plasma from whole blood using planar microfilters for lab-on-a-chip applications," Lab Chip **5**, 922–929 (2005).

[16] A. Ehrenhofer, G. Bingel, G. Paschew, M. Tietze, R. Schröder, A. Richter, and T. Wallmersperger, "Permeation control in hydrogel-layered patterned PET membranes with defined switchable pore geometry—Experiments and numerical simulation," Sens. Actuators, B **232**, 499–505 (2016).

[17] S. Maury, "The antiproton decelerator: AD," Hyperfine Interact. **109**, 43–52 (1997).

[18] C. Smorra, S. Sellner, M. Borchert, J. Harrington, T. Higuchi, H. Nagahama, T. Tanaka, A. Mooser, G. Schneider, M. Bohman, K. Blaum, Y. Matsuda, C. Ospelkaus, W. Quint, J. Walz, Y. Yamazaki, and S. Ulmer, "A parts-per-billion measurement of the antiproton magnetic moment," Nature **550**, 371–374 (2017).

[19] M. Borchert, J. Devlin, S. Erlewein, M. Fleck, J. Harrington, T. Higuchi, B. Latacz, F. Voelksen, E. Wursten, F. Abbass, M. A. Bohman, A. H. Mooser, D. Popper, M. Wiesinger, C. Will, K. Blaum, Y. Matsuda, C. Ospelkaus, W. Quint, J. Walz, Y. Yamazaki, C. Smorra, and S. Ulmer, "A 16-parts-per-trillion measurement of the antiproton-to-proton charge–mass ratio," Nature **601**, 53–57 (2022).

[20] S. Sellner, M. Besirli, M. Bohman, M. Borchert, J. Harrington, T. Higuchi, A. Mooser, H. Nagahama, G. Schneider, C. Smorra, T. Tanaka, K. Blaum, Y. Matsuda, C. Ospelkaus, W. Quint, J. Walz, Y. Yamazaki, and S. Ulmer, "Improved limit on the directly measured antiproton lifetime," New J. Phys. **19**, 083023 (2017).

[21] X. Fei, "Trapping low energy antiprotons in an ion trap," Ph.D. thesis, Harvard University, Department of Physics, 1990.

[22] D. Kuchler, M. Paoluzzi, M. Hori, T. Eriksson, F. Pedersen, G. Vanbavinckhove, B. Puccio, S. Maury, S. Fedemann, J. Harasimowicz *et al.*, "Extra low energy antiproton (ELENA) ring and its transfer lines: Design report," Tech. Rep., CERN, 2014.

[23] J. Engel, M. Gross, G. Koss, O. Lishilin, G. Loisch, S. Philipp, D. Richter, and F. Stephan, "Polymer foil windows for gas–vacuum separation in accelerator applications," AIP Adv. **10**, 025224 (2020).

[24] M. Mapes, H. Hseuh, and W. Jiang, "Permeation of argon, carbon dioxide, helium, nitrogen, and oxygen through Mylar windows," J. Vac. Sci. Technol. A **12**, 1699–1704 (1994).

[25] W. Hassenzahl and W. Gray, "Thin windows for gaseous and liquid targets: An optimization procedure," Cryogenics **15**, 627–638 (1975).

[26] Apiezon, "Ultra high and high vacuum greases," https://static.mimaterials.com/apiezon/DocumentLibrary/TechnicalDatasheets/Apiezon_L_M_and_N_Ultra_High_and_High_Vacuum_Greases_Datasheet.pdf (accessed 21 July 2022).

[27] J. Ružbarský, *Contactless System for Measurement and Evaluation of Machined Surfaces* (Springer, 2022).

[28] R. Gruen, "Process and apparatus for coating conducting pieces using a pulsed glow discharge," US Patent 5,015,493 (1991).

[29] H. Klauk, *Organic Electronics: Materials, Manufacturing, and Applications* (John Wiley & Sons, 2006).

[30] A. Fuoco, B. Comesaña-Gándara, M. Longo, E. Esposito, M. Monteleone, I. Rose, C. G. Bezzu, M. Carta, N. B. McKeown, and J. C. Jansen, "Temperature

dependence of gas permeation and diffusion in triptycene-based ultrapermeable polymers of intrinsic microporosity," ACS Appl. Mater. Interfaces **10**, 36475–36482 (2018).
[31]S. P. Møller, A. Csete, T. Ichioka, H. Knudsen, U. Uggerhøj, and H. Andersen, "Antiproton stopping at low energies: Confirmation of velocity-proportional stopping power," Phys. Rev. Lett. **88**, 193201 (2002).
[32]J. F. Ziegler, M. D. Ziegler, and J. P. Biersack, "SRIM—The stopping and range of ions in matter (2010)," Nucl. Instrum. Methods Phys. Res., Sect. B **268**, 1818–1823 (2010).
[33]D. Thwaites, "Bragg's rule of stopping power additivity: A compilation and summary of results," Radiat. Res. **95**, 495–518 (1983).
[34]K. Nordlund, M. Hori, and D. Sundholm, "Large nuclear scattering effects in antiproton transmission through polymer and metal-coated foils," Phys. Rev. A **106**, 012803 (2022).
[35]smarAct, Note1, smarAct SLC-1730-CR-UHVP-NM-TI, smarAct (accessed 21 July).
[36]M. Kretzschmar, "Calculating damping effects for the ion motion in a penning trap," Eur. Phys. J. D **48**, 313–319 (2008).